

# Introduction to Dark matter and Direct detection principles

by

**Praveen Sharma**

M. Sc. Student, Department of Physics  
Indian Institute of Technology Guwahati  
Guwahati-781039, Assam  
IAS-INSA-NASI Summer Research Fellow, 2018

Under the guidance of

**Prof. Bedangadas Mohanty**

School of Physical Sciences  
National Institute of Science Education and Research(NISER)  
Jatni, Khurda - 752050, Odisha



## **Abstract**

There is overwhelming evidence that approximately 85% of the matter in the universe is non-luminous, nonbaryonic, cold (nonrelativistic) and unknown, termed as “dark matter”. This is based on observations like rotation curves of galaxies, gravitational lensing effects, extensive analysis of the cosmic microwave background etc. While dark matter has not been detected as of yet, a class of dark matter particles referred to as Weakly Interacting Massive Particles (WIMPs) has been established as the leading candidate. The existence of WIMPs naturally arises from many extensions of the standard particle physics model like Supersymmetry or Universal Extra Dimensions. There are three different strategies for WIMP detection, namely Indirect Detection, Collider Search and Direct Detection. In Direct Detection experiments, WIMPs are expected to have collapsed into a roughly isothermal, spherical halo within which the visible portion of our galaxy resides. They would scatter off target nuclei in the weak interaction scale, potentially allowing their direct detection. These direct detection experiments are designed to search for WIMPs elastically scattering the target nuclei. The regime of the signal makes this approach an extremely challenging endeavour since the expected event rate is immensely small, it could be one event/ton/year or even less. In this report I will present a systematic derivation and discussion of the practical formulae needed to design and interpret direct searches for nuclear recoil events caused by WIMPs assuming that there is spin independent WIMP-Nucleon Elastic Scattering. Further, for an experiment what experimenters report is an upper limit on the WIMP interaction cross section if the signal they are trying to detect is non-existent or below their experiment’s sensitivity. This is called an exclusion plot, and the limits on the WIMP interaction cross section are set by calculating the upper confidence limit on the theoretical event rate, discussion of which will be included in the report.

# Contents

<b>1</b>	<b>The Dark Matter quest</b>	<b>2</b>
1.1	Dark Matter evidences . . . . .	2
1.1.1	Galactic Scale . . . . .	2
1.1.2	The Scale of Galaxy Clusters . . . . .	3
1.1.3	Cosmological Scales . . . . .	5
1.2	Dark Matter Properties . . . . .	7
1.3	Weakly Interacting Massive Particles (WIMPs) . . . . .	9
1.4	Strategies for WIMP detection . . . . .	10
<b>2</b>	<b>Direct detection of dark matter</b>	<b>12</b>
2.1	Kinematics of WIMP-Nucleus Elastic Scattering . . . . .	12
2.2	Standard Halo Model . . . . .	16
2.3	Expected Event Rate . . . . .	19
2.4	WIMP-Nucleon cross section . . . . .	24
2.5	Nuclear Form Factor . . . . .	25
2.6	Correction in event rate due to Earth's velocity . . . . .	29
2.7	Direct Detection techniques . . . . .	32
<b>3</b>	<b>Dark Matter exclusion limits</b>	<b>34</b>
3.1	Poisson Method . . . . .	35
3.2	Maximum Gap method . . . . .	35
3.2.1	Result . . . . .	39

# Chapter 1

## The Dark Matter quest

### 1.1 Dark Matter evidences

#### 1.1.1 Galactic Scale

The most convincing and direct evidence for dark matter on galactic scales comes from the observations of the rotation curves of galaxies, namely the graph of circular velocities of stars and gas as a function of their distance from the galactic center.

Rotation curves are usually obtained by combining observations of the 21cm line with optical surface photometry. Observed rotation curves usually exhibit a characteristic flat behavior at large distances (done by Vera Rubin[4] [5]), i.e. out towards, and even far beyond, the edge of the visible disks (example in Fig 1.1).

In Newtonian dynamics the circular velocity is expected to be

$$v(r) = \sqrt{\frac{GM(r)}{r}}$$

where  $M(r) = 4\pi \int \rho(r)r^2 dr$  and  $\rho(r)$  is the mass density profile.

To explain a rotation curve that does not change as a function of radius, as before we balance gravity and the centripetal force, but now we assume a constant circular velocity,  $v_c$ . So:

$$\frac{mv_c^2}{r} = \frac{GM(r)m}{r^2} \rightarrow M(r) = \frac{v_c^2 r}{G}$$

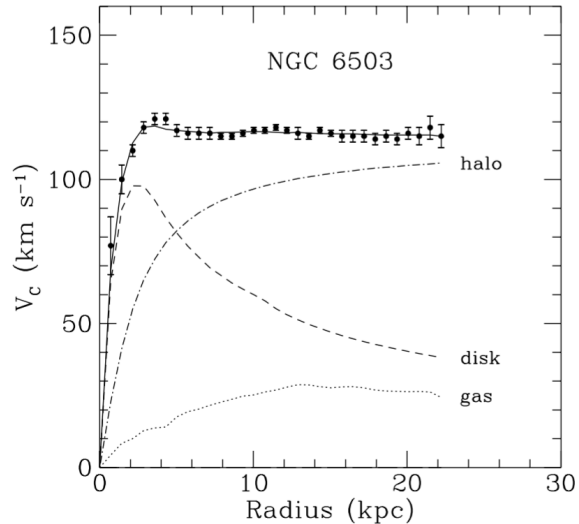


**Figure 1.1:** Measured rotation curve of the spiral galaxy NGC 6503 (solid). The dashed and the dotted curves represent the contributions from the visible part of the galaxy and the gas within the galaxy respectively. The dashed-dotted curve denotes the inferred contribution from the dark matter halo, which is needed to explain the observation. Figure taken from [6]

In this equation  $M(r)$  represents the mass within a radius  $r$ . The density corresponding to this mass distribution is given by:

$$\rho(r) = \frac{v_c^2}{4\pi G} \frac{1}{r^2}$$

Therefore, the fact that  $v(r)$  is approximately constant implies the existence of an halo with  $M(r) \propto r$  and  $\rho(r) \propto 1/r^2$ .

It is important to note that if we would integrate such a mass distribution to infinitely large  $r$  the mass of a galaxy becomes infinitely large! So even though the constant orbital velocity of spiral galaxies is observed to arbitrarily large radii, at some point there should be a hard cut-off of some kind.

### 1.1.2 The Scale of Galaxy Clusters

A cluster of galaxies gave the first hints of dark matter (in the modern sense). In 1933, Fritz Zwicky studied the peculiar motions of galaxies in the Coma cluster [1][2]. Assuming that the galaxy cluster is an isolated system, the virial theorem

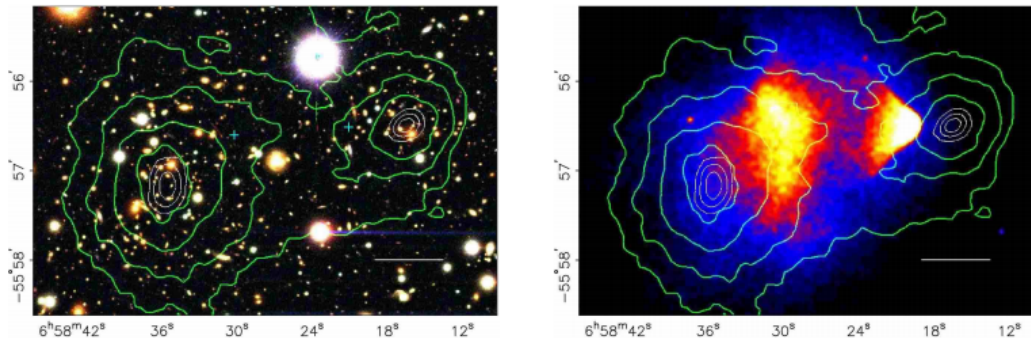


**Figure 1.2:** Images of the Bullet Cluster. An optical photograph from the Hubble Space Telescope is shown on the left and an X-ray image from the Chandra X-Ray Observatory is shown on the right. The overlaid lines represent contours of the mass distribution, obtained from an analysis based on gravitational lensing. Figure taken from [12]

can be used to relate the average velocity of objects with the gravitational potential (or the total mass of the system). The results was an extremely large mass-to-light ratio, indicative of the existence of large amounts of missing mass, which can be attributed to a DM component.

The mass of a cluster can be determined via several methods, including application of the virial theorem to the observed distribution of radial velocities, by weak gravitational lensing, and by studying the profile of X-ray emission that traces the distribution of hot emitting gas in rich clusters.

### **Bullet Cluster :**

The Bullet Cluster (1E 0657-558)[12] is a paradigmatic example of the effect of dark matter in dynamical systems. It consists of two galaxy clusters which underwent a collision. The collision was analyzed based on observations of X-rays, which trace the visible baryonic matter, and applying techniques based on gravitational lensing, which map the distribution of the total mass dominated by dark matter. A clear separation between the visible matter and the dark matter is apparent from Fig. The dark matter halos passed through each other, while the baryonic matter decelerated and dragged behind the dark matter due to electromagnetic interactions. The Bullet Cluster is considered one of the best arguments against MOND theories (since the gravitational effects occur where there is no visible matter). It also sets an upper bound on the self-interaction strength of dark matter particles [11].

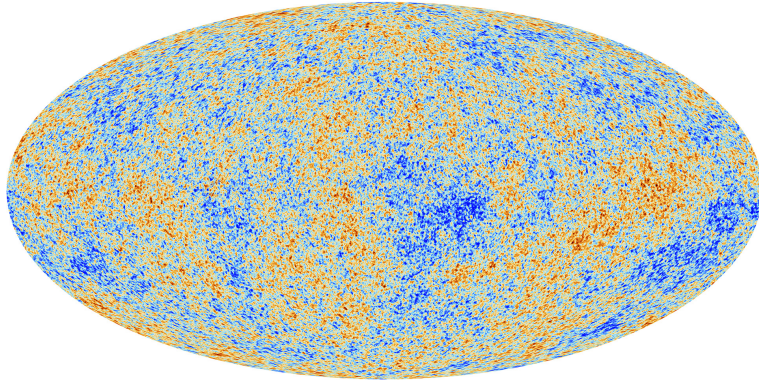


**Figure 1.3:** Temperature anisotropies of the cosmic microwave background from Planck 2015. Fig taken from [17]

### 1.1.3 Cosmological Scales

On distance scales of the size of galaxies and clusters of galaxies, evidence of dark matter appears to be compelling. Despite this, the observations discussed do not allow us to determine the total amount of dark matter in the Universe. Such information can be extracted from the analysis of the Cosmic Microwave Background (CMB).

The existence of background radiation originating from the propagation of photons in the early Universe (once they decoupled from matter) was predicted by George Gamow and his collaborators in 1948 and inadvertently discovered by Arno Penzias and Robert Wilson in 1965. After many decades of experimental effort, the CMB is known to be isotropic at the  $10^5$  level and to follow with extraordinary precision the spectrum of a black body corresponding to a temperature  $T = 2.726K$ .

The analysis of CMB anisotropies enables accurate testing of cosmological models and puts constraints on cosmological parameters. The observed temperature anisotropies in the sky are usually expanded as

$$\frac{\delta T}{T}(\theta, \phi) = \sum_{l=2}^{\infty} \sum_{m=-l}^l a_{lm} Y_{lm}(\theta, \phi)$$

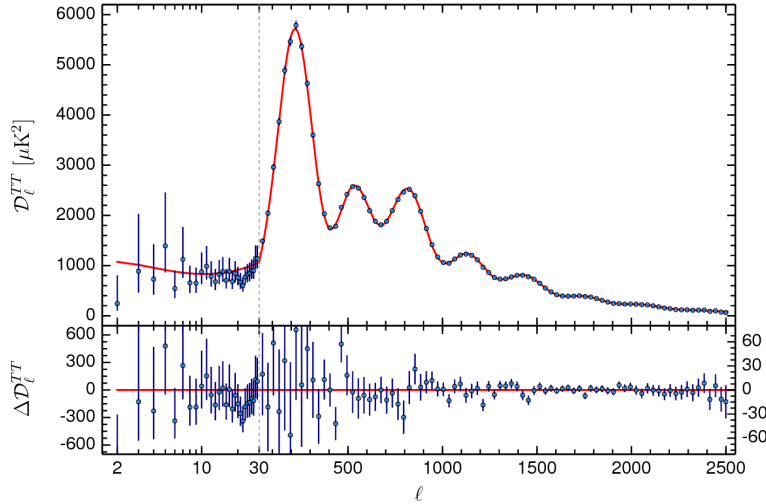


**Figure 1.4:** Power spectrum of the temperature anisotropies of the cosmic microwave background from Planck 2015. Figure taken from [17]

where  $Y_{lm}(\theta, \phi)$  are spherical harmonics. The variance  $C_l$  of  $a_{lm}$  is given by

$$C_l = \langle |a_{lm}|^2 \rangle = \frac{1}{2l+1} \sum_{m=-l}^l |a_{lm}|^2$$

If the temperature fluctuations are assumed to be Gaussian, as appears to be the case, all of the information contained in CMB maps can be compressed into the power spectrum, essentially giving the behavior of  $C_l$  as a function of  $l$ .

The methodology, for extracting information from CMB anisotropy maps, is simple, at least in principle. Starting from a cosmological model with a fixed number of parameters (usually 6 or 7), the best-fit parameters are determined.

The size and the position of the peaks of the CMB spectrum, Figure 1.4, provide valuable information on cosmological parameters, such as the curvature and energy matter composition of the universe:  $\Omega_{tot}$ ,  $\Omega_b$  and  $\Omega_{DM}$ . From the CMB study [16][10] it is then possible to extract an estimate of the non-baryonic Dark Matter abundance in the Universe:

$$\Omega_\Lambda = 0.707 \pm 0.010;$$

$$\Omega_m = 0.293 \pm 0.056 \pm 0.010;$$

$$\Omega_b h^2 = 0.02211 \pm 0.00034;$$

$$\Omega_{DM} h^2 = 0.1162 \pm 0.0020$$

From the values of the cosmological parameters it is clear that the dark energy ( $\Lambda$ ) accounts for about 70% of the Universe energy content while the majority of the matter content is in the form of non-baryonic dark matter. The abundance of the baryonic matter is also in agreement with what expected from the BBN, which is another strong point in favor of the DM existence.

## 1.2 Dark Matter Properties

- **Neutral**

It is generally argued that DM particles must be electrically neutral. Otherwise they would scatter light and thus not be dark.

- **Nonrelativistic**

Numerical simulations of structure formation in the Early Universe have become a very useful tool to understand some of the properties of dark matter. In particular, it was soon found that dark matter has to be non-relativistic (cold) at the epoch of structure formation.

Relativistic (hot) dark matter has a larger free-streaming length (the average distance traveled by a dark matter particle before it falls into a potential well). This leads to inconsistencies with observations. However, at the Galactic scale, cold dark matter simulations lead to the occurrence of too much substructure in dark matter haloes. Apparently this could lead to a large number of subhaloes (observable through the luminous matter that falls into their potential wells). It was argued that if dark matter was warm (having a mass of approximately 2-3 keV) this problem would be alleviated. Modern simulations, where the effect of baryons is included, are fundamental in order to fully understand structure formation in our Galaxy and determine whether dark matter is cold or warm. For further references see <http://https://www.youtube.com/watch?v=ScuA0Cvmp4o>

- **NonBaryonic**

The results of the CMB, together with the predictions from Big Bang nucle-

osynthesis, suggest that only 4-5% of the total energy budget of the universe is made out of ordinary (baryonic) matter. Given the mismatch of this with the total matter content, we must conclude that DM is non-baryonic.

Neutrinos: Neutrinos deserve special mention in this section, being the only viable nonbaryonic DM candidate within the SM. Neutrinos are very abundant particles in the Universe and they are known to have a (very small) mass. Given that they also interact very feebly with ordinary matter (only through the electroweak force) they are in fact a component of the DM. There are, however various arguments that show that they contribute in fact to a very small part.

First, neutrinos are too light. Through the study of the decoupling of neutrinos in the early universe we can compute their thermal relic abundance. Using current upper bounds on the neutrino mass, we obtain  $\Omega_\nu h^2 < 0.003$ , a small fraction of the total DM abundance.

Second, neutrinos are relativistic (hot) at the epoch of structure formation. As mentioned above, hot DM leads to a different hierarchy of structure formation at large scales, with large objects forming first and small ones occurring only after fragmentation. This is inconsistent with observations.

- **Long-Lived**

Possibly the most obvious observation is that DM is a long-lived (if not stable) particle. The footprint of DM can be observed in the CMB anisotropies, its presence is essential for structure formation and we can feel its gravitational effects in clusters of galaxies and galaxies nowadays.

Stable DM candidates are common in models in which a new discrete symmetry is imposed by ensuring that the DM particle is the lightest with an exotic charge (and therefore its decay is forbidden). This is the case, e.g., in Supersymmetry (when R-parity is imposed), Kaluza-Klein scenarios (K-parity) or little Higgs models.

However, stability is not required by observation. DM particles can decay, as long as their lifetime is longer than the age of the universe. Long-lived DM particles feature very small couplings. Characteristic examples are gravitinos (whose decay channels are gravitationally suppressed) or axinos (which decays through the axion coupling).

- **Collisionless**

Dynamical systems, such as cluster collisions, set an upper bound to the self-interactions of DM particles. Observations seem to suggest that the DM component in these objects is mostly collision-less, thus behaving very differently than ordinary matter. Dark matter’s lack of deceleration in the bullet cluster constrains its self-interaction cross-section  $\sigma/m < 1.25\text{cm}^2\text{g}^{-1} \approx 2\text{b GeV}^{-1}$ .

### 1.3 Weakly Interacting Massive Particles (WIMPs)

Going beyond the standard model, dark matter particles are identified with the general definition of: Weakly Interacting Massive Particles (WIMPs). They are stable, cold, non-baryonic and interact only through gravitational and weak forces. There are several WIMP candidates raising, for example, from Supersymmetry; the most promising among them is lightest supersymmetric particle (LSP), the neutralino.

If WIMPs are stable, there is a cosmological relic abundance produced during the Big Bang. Assuming for such particles a mass  $m_\chi$ , one has that for  $T > m_\chi$  they were in thermal equilibrium while at temperatures below  $m_\chi$  they decoupled and their abundance started to lower. Finally, when the expansion rate of the Universe became larger than the annihilation rate ( $\Gamma < H$ , where  $H$  is the Hubble constant), the WIMP abundance “frozen out”, resulting in the current relic abundance. A thorough discussion of the Boltzmann equation and the relic density of neutralino is given in [20][8].

The evolution of the WIMP density is described by the Boltzmann equation:

$$\frac{dn}{dt} + 3Hn_\chi = -\langle\sigma_a v\rangle[(n_\chi)^2 - (n_\chi^{eq})^2]$$

where  $n_\chi^{eq}$  is the number density at the thermal equilibrium and  $\langle\sigma_a v\rangle$  is the thermally averaged total annihilation cross section. For massive particles (non-relativistic limit) and in the Maxwell-Boltzmann approximation,  $n_\chi^{eq}$  is given by:

$$n_\chi^{eq} = g \left( \frac{m_\chi T}{2\pi} \right)^{3/2} e^{-m_\chi/T}$$

where  $g$  is the number of degree of freedom,  $m_\chi$  is the particle mass and  $T$  is the temperature. The "freeze out" is verified for  $\Gamma = H$  that results in a temperature  $T = m_\chi/20$ . Introducing the entropy density  $s = 2\pi^2 g_* T^3/45$ , where  $g_*$  counts the number of relativistic degrees of freedom, and using the conservation of entropy per co-moving volume one has:

$$\left(\frac{n_\chi}{s}\right)_0 = \left(\frac{n_\chi}{s}\right)_f = \frac{H(T_f)}{\langle\sigma_{av}\rangle s(T_f)} = 100 \frac{1}{g_*^{1/2} m_\chi m_{Pl} \langle\sigma_{av}\rangle}$$

where  $m_{Pl}$  is the Planck mass and the subscripts 0 and  $f$  denote the present and the freeze-out epoch, respectively. Thus, the relic density can be expressed as function of the annihilation rate:

$$\Omega_\chi h^2 = \frac{m_\chi n_\chi}{\rho_c} = 3 \times 10^{27} \frac{\text{cm}^3 \text{s}^{-1}}{\langle\sigma_{av}\rangle}$$

that is independent from  $m_\chi$ . The annihilation cross section of a new particle interacting at the weak scale can be estimated as:  $\langle\sigma_{av}\rangle \propto 10^{-25} \text{cm}^3 \text{s}^{-2}$ . This value is close to that derived from cosmological arguments which strongly suggests that if a stable particle associated with the electro-weak scale interactions exists, then it is likely to be the dark matter particle. This coincidence has provided strong motivation for finding WIMPs.

## 1.4 Strategies for WIMP detection

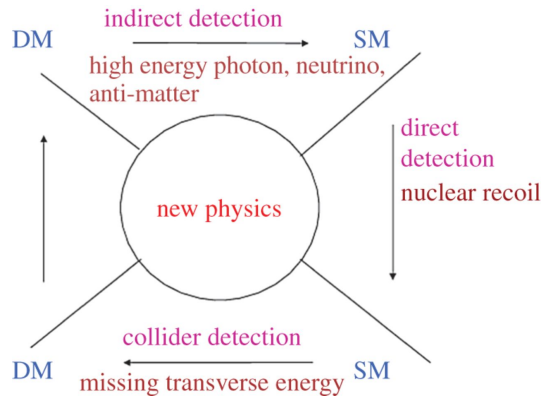


**Figure 1.5:** Feynman diagram for searching DM

DM particles are probed by following methods:

- **Direct Detection ( $\text{DM} + \text{SM} \rightarrow \text{DM} + \text{SM}$ ):** measure recoil energy ( $\sim \text{eV-keV}$ ) by DM scattering off targets in detectors on Earth. Various experiments are : superCDMS, COUPP, CoGeNT, CRESST, PICASSO, LUX, ZEPLIN, XENON100, PICO etc.
- **Indirect Detection ( $\text{DM} + \text{DM} \rightarrow \text{SM} + \text{SM}$ ):** measure gamma rays, neutrinos , positrons, antiprotons, anti-deuterons, etc. from DM annihilation in Galactic centre, in Sun, in Milky way. Various experiments are : Fermi-LAT, IceCube, PAMELA, AMS-02 etc.
- **Collider Search ( $\text{SM} + \text{SM} \rightarrow \text{DM} + \text{DM}$ ):** Produce DM by colliding two SM particles or by decay of SM particles and infer about DM from missing energy.

# Chapter 2

## Direct detection of dark matter

### 2.1 Kinematics of WIMP-Nucleus Elastic Scattering

For an accurate description of the WIMP scattering to a nucleus, an understanding of the kinematics involved in the collision is needed. First, assume that the target nuclei involved in a collision with a WIMP is not moving, while the WIMP approaches the nucleus with a velocity  $v$ .

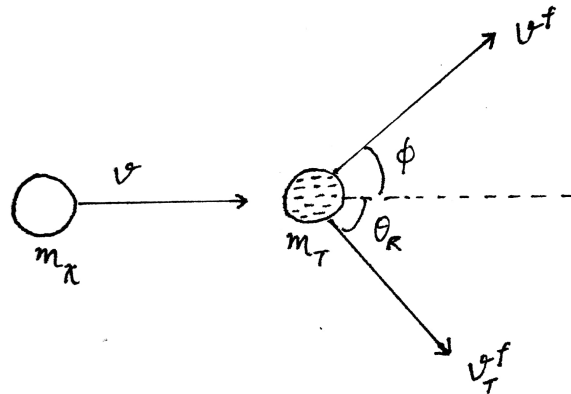


Figure 2.1: WIMP-Nucleus elastic collision in Lab frame

In Lab frame, after the collision, the amount of energy imparted to the nucleus

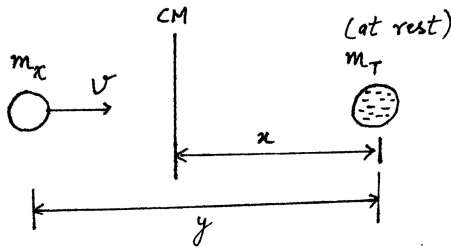
(recoil energy) by the WIMP is given by,

$$E_R = \frac{1}{2}m_T(v_T^f)^2 = \frac{1}{2}m_T((v_{T_x}^f)^2 + (v_{T_y}^f)^2) \quad (2.1)$$

where  $m_T$  is the mass of target nucleus and  $v_T^f$  is the velocity of the nucleus after the collision.

Looking at the problem in the CM frame:

The first step is to find velocity  $v_{cm}$  of the centre of mass frame for a WIMP colliding with a nucleus, relative to the nucleus.



$$\begin{aligned} m_T x &= m_\chi (y - x) \\ (m_T + m_\chi)x &= m_\chi y \\ v_{cm} &= \frac{dx}{dt} = \frac{m_\chi}{m_\chi + m_T} \frac{dy}{dt} \\ v_{cm} &= \frac{m_\chi}{m_\chi + m_T} v \end{aligned} \quad (2.2)$$

The second step is to find momentum of each particle to an observer in the CM frame.

Target Nucleus : Moves at velocity  $-v_{cm}$  so momentum is  $-m_T v_{cm}$ , i.e.

$$p_i^T = -m_T v_{cm}$$

WIMP : Moves at velocity  $v - v_{cm}$  so its momentum is  $m_\chi (v - v_{cm})$ , i.e.

$$\begin{aligned} p_i^\chi &= m_\chi (v - v_{cm}) \\ &= m_\chi v \left( 1 - \frac{m_\chi}{m_\chi + m_T} \right) \\ &= m_T \frac{m_\chi}{m_\chi + m_T} v \\ &= m_T v_{cm} \end{aligned}$$

Therefore in CM frame, momentum of WIMP and target nucleus are equal in magnitude and opposite in sign, i.e.  $|p_i^T| = |p_i^\chi| = p_i$ .

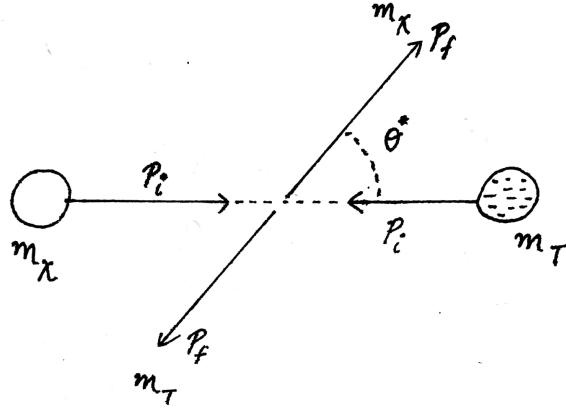


**Figure 2.2:** WIMP-Nucleus elastic collision in Centre of mass frame

Defining the reduced mass of the WIMP and Target:

$$\mu = \frac{m_\chi m_T}{(m_\chi + m_T)} \quad \text{so that} \quad v_{cm} = \frac{m_\chi}{m_\chi + m_T} v = \frac{\mu v}{m_T} \quad (2.3)$$

and  $p_i = \mu v$

Using conservation of energy in CM frame:

$$\frac{p_i^2}{2m_\chi} + \frac{p_i^2}{2m_T} = \frac{p_f^2}{2m_\chi} + \frac{p_f^2}{2m_T}$$

which implies  $p_i = p_f$

Therefore, In the CM frame, the magnitude of momentum stays the same.

Final state velocities in CM frame:

We are interested in the velocity of the target nucleus after the collision. Its momentum after the collision in the CM frame has the same magnitude as it did before the collision. So its velocity resolves into two components, still in the CM frame, one parallel to the incident direction of the WIMP and the other perpendicular. In this frame the initial velocity of the target is  $v_{cm}$  in the  $-x$  direction. Therefore its final velocity has these components with  $\theta^*$  as the scattering angle in centre of mass frame:

horizontal CM frame:  $(v_{T_x}^f)_C = v_{cm} \cos \theta^*$

$$\text{verticle CM frame: } (v_{T_y}^f)_C = v_{cm} \sin \theta^*$$

Returning to the lab frame, horizontal and vertical component of the velocity of target after collision can be found by subtracting the centre of mass velocity  $v_{cm}$  from the  $x$  component of the target velocity:

$$\begin{aligned} (v_{T_x}^f)_L &= v_{cm} \cos \theta^* - v_{cm} \\ (v_{T_y}^f)_L &= v_{cm} \sin \theta^* \end{aligned} \quad (2.4)$$

Since what is needed is the amount of energy imparted (in the LAB frame) to the nucleus by the WIMP ( $E_R$ ). Therefore, using equations (2.3) and (2.4) in equation (2.1)

$$\begin{aligned} E_R &= \frac{1}{2} m_T ((v_{T_x}^f)_L^2 + (v_{T_y}^f)_L^2) \\ &= \frac{1}{2} m_T v_{cm}^2 ((\cos \theta^* - 1)^2 + (\sin \theta^*)^2) \\ &= m_T v_{cm}^2 (1 - \cos \theta^*) \\ &= \frac{\mu^2 v^2}{m_T} (1 - \cos \theta^*) \end{aligned} \quad (2.5)$$

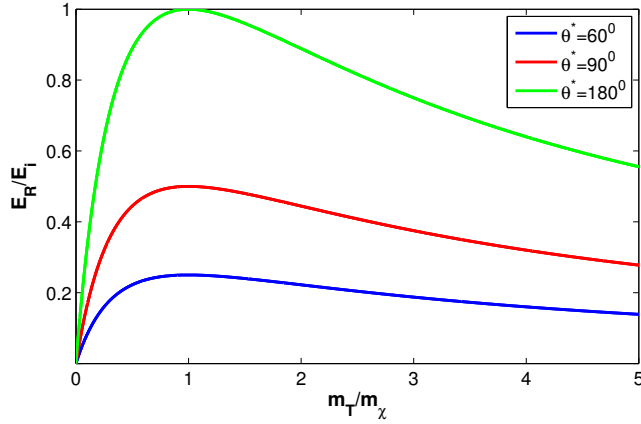


**Figure 2.3:** Fraction of energy imparted to the nucleus by WIMP vs target to WIMP mass ratio for different scattering angle.

Equation (2.5) can also be written in other form:

$$E_R = \left( \frac{1}{2} m_\chi v^2 \right) \left( \frac{4m_\chi m_T}{(m_\chi + m_T)^2} \right) \left( \frac{1 - \cos \theta^*}{2} \right) \quad (2.6)$$

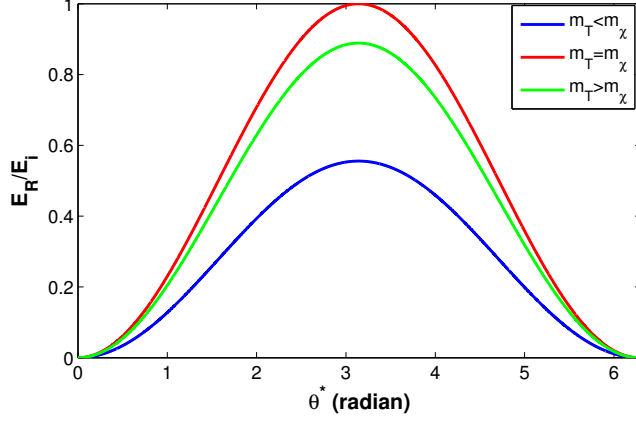


**Figure 2.4:** Fraction of energy imparted to the nucleus by WIMP vs scattering angle ( $\theta^*$ ) for different target to WIMP mass ratio.

The first term on the right is the energy of the incoming WIMP ( $E_i$ ) and the second term is the kinematic factor  $r$  ( $0 < r < 1$ ). Therefore,

$$E_R = E_i r \frac{(1 - \cos \theta^*)}{2} \quad (2.7)$$

The fraction of incoming WIMP's energy imparted to the target nucleus ( $E_R/E_i$ ) as a function of target to WIMP mass ratio ( $m_T/m_\chi$ ) for different scattering angle ( $\theta^*$ ) is shown in Figure 2.3. It is observed that, for a given  $\theta^*$ , fraction of imparted energy is maximum when mass ratio = 1, i.e  $m_T = m_\chi$ . Also, for a given mass ratio, maximum WIMP's energy is transferred to target nucleus for  $\theta^* = 180^\circ$ , i.e for a head on collision.

In Figure 2.4, fraction of energy imparted to the nucleus by WIMP vs scattering angle ( $\theta^*$ ) for different target to WIMP mass ratio is shown. Again it is observed that, for a given mass ratio fraction of imparted energy is maximum when scattering angle is  $180^\circ$  (head on collision). Also, for a particular scattering angle maximum energy is imparted when  $m_T = m_\chi$ .

## 2.2 Standard Halo Model

Most of direct detection signal calculations and data analyses have used the Standard Halo Model (SHM) to model the WIMP velocity distribution. The model assumes an isothermal and isotropic sphere of an ideal WIMP gas with density profile  $\rho(r) \propto 1/r^2$ . The velocity distribution corresponding to this density, in the

galactic rest frame is assumed to be Maxwellian:

$$f(v) = Ne^{-v^2/2\sigma_v^2}$$

where  $\sigma_v$  is the velocity dispersion. With this assumption I will prove that the corresponding density behaves like  $1/r^2$ . From statistical mechanical arguments there are a few statements which can be made. The first one is relating the average kinetic energy  $\langle K \rangle$  and thus the mean square speed  $\langle v^2 \rangle$  of the dark matter particles to their temperature:

$$\langle K \rangle = \frac{1}{2}m\langle v^2 \rangle = \frac{3}{2}k_B T \implies \langle v^2 \rangle = \frac{3k_B T}{m}$$

Here  $m$  represents the mass of a hypothetical dark matter particle,  $T$  is the temperature and  $k_B$  is Boltzmann's constant.

It can be derived easily that the average square velocity corresponding to a Maxwellian distribution is given by:

$$\langle v^2 \rangle = 3\sigma_v^2$$

comparing above two results we get,

$$\sigma_v = \sqrt{\frac{k_B T}{m}}$$

The next step is looking at the equation of state. For an ideal collisionless gas we know the equation of state:

$$pV = nk_B T \implies p(r) = \rho(r) \frac{k_B T}{m} = \sigma_v^2 \rho(r)$$

Now assuming that hydrostatic pressure balances the gravitational collapse,

$$\frac{dp}{dr} = -\rho(r) \frac{GM(r)}{r^2} \implies \sigma_v^2 \frac{d\rho}{dr} = -\rho(r) \frac{GM(r)}{r^2}$$

Multiplying both sides of the equation by  $r^2/\rho\sigma_v^2$ , leads to:

$$\frac{r^2}{\rho} \frac{d\rho}{dr} = -\frac{GM(r)}{\sigma_v^2}$$

Differentiating w.r.t  $r$  gives

$$\frac{d}{dr} \left( r^2 \frac{d}{dr} \log \rho \right) = -\frac{G}{\sigma_v^2} \frac{dM(r)}{dr}$$

using

$$\frac{dM(r)}{dr} = 4\pi r^2 \rho(r)$$

we get

$$\frac{d}{dr} \left( r^2 \frac{d}{dr} \log \rho \right) = -\frac{4\pi G}{\sigma_v^2} r^2 \rho$$

Solving above equation gives:

$$\rho(r) = \frac{\sigma_v^2}{2\pi G} \frac{1}{r^2}$$

comparing this density with observed density profile from rotation curves:

$$\rho(r) = \frac{\sigma_v^2}{2\pi G} \frac{1}{r^2} = \frac{v_c^2}{4\pi G} \frac{1}{r^2}$$

Therefore in order to describe rotation curves following relation must hold:

$$2\sigma_v^2 = v_c^2$$

The orbital velocity at the sun's distance from the galactic center has already reached the constant value, so  $v_c(r \rightarrow \infty) = v_0 = \sqrt{2}\sigma_v$ , where  $v_0$  is called the characteristic velocity. The dark matter particle velocity distribution can now be written as:

$$f(v) = N e^{-v^2/v_0^2}$$

Now, in order to use it for direct detection experiments we need to carry out a Galilean transformation, i.e the velocity distribution must be boosted from the halo frame to the lab (Earth) frame. This is done by

$$v \rightarrow v + v_E$$

such that

$$f(v, v_E) \propto e^{-(v+v_E)^2/v_0^2} \quad (2.8)$$

where  $v_E$  is the velocity of the Earth with respect to the galactic rest frame.

$$v_E = v_{LSR} + v_{\odot} + v_{\oplus}$$

$v_E$  includes contributions from the speed of the Local Standard of Rest  $v_{LSR}$ . This corresponds to the Galactic circular rotation at the Earth's radius  $R_0$ .  $v_{\odot}$  is the peculiar velocity of the Sun with respect to  $v_{LSR}$ , and  $v_{\oplus}$  is the Earth's orbital velocity around the sun. SHM assumes the rotation curve of the galaxy has already reached its asymptotic value at  $R_0$  giving  $v_0 = v_{LSR}$ . By this argument, the most probable velocity of the WIMPs is identical to the LSR in the SHM.

Also, the pure Maxwellian velocity distribution extends to infinite velocities, but in a physical picture the distribution will be cut off at some maximum velocity. In the frame of the halo, this maximum velocity is the Galactic escape velocity ( $v_{esc}$ ).

The values adopted in the SHM for the astrophysical quantities defined above along with local dark matter density ( $\rho_{\chi}$ ) is shown in Table 2.1 [18].

Constant	Symbol	SHM value
Characteristic Velocity	$v_0$	220 km s <sup>-1</sup>
Solar Peculiar Velocity	$v_{\odot}$	12.2 km s <sup>-1</sup>
Earth Orbital Velocity	$v_{\oplus}$	29.8 km s <sup>-1</sup>
Galactic Escape Velocity	$v_{esc}$	544 km s <sup>-1</sup>
Local Dark Matter Density	$\rho_{\chi}$	0.3 GeV c <sup>-2</sup> cm <sup>-3</sup>

**Table 2.1:** Astrophysical constants and their values in the Standard Halo Model.

## 2.3 Expected Event Rate

First step is to calculate event rates that could be observed in an experimental setup. From the event rates we will be able to get an idea about what are the requirements that a dark matter detector will have to fulfill.

In this section all the pieces will be put together to calculate the nuclear recoil rate as a function of recoil energy,  $E_R$ . Since we know from the previous section that:

$$E_R = E_i r \frac{(1 - \cos \theta^*)}{2}$$

Starting with the important assumption that the scattering of the WIMPs to nuclei is isotropic, i.e. there is no preferred angle in the center of mass frame, so that the

recoils are uniformly distributed in  $E_R$ , over the range:

$$0 \leq E_R \leq E_i r$$

The differential rate  $\frac{dR(E_R)}{dE_R}$  in terms of  $E_R$  can then be written as:

$$d \left( \frac{dR(E_R)}{dE_R} \right) = \frac{dR(E_i)}{E_i r}$$

In this equation  $dR(E_i)$  represents the rate of nuclear recoils within an energy range between  $E_i$  and  $E_i + dE_i$ . The next step is to integrate over all the possible values of the incoming energy that can cause a recoil energy  $E_R$ .

$$\frac{dR}{dE_R} = \int_{E_{min}}^{E_{max}} \frac{1}{E_i r} dR(E_i) \quad (2.9)$$

where  $E_{min}$  is the minimal energy which is required to give a recoil energy  $E_R$ .

$$E_{min} = \frac{E_R}{r}$$

From which we can derive the corresponding minimal velocity:

$$E_{min} = \frac{1}{2} m_\chi v_{min}^2 \Rightarrow v_{min} = \left( \frac{2E_R}{m_\chi r} \right)^{1/2}$$

Now, defining the most probable energy of WIMP as :

$$E_0 = \frac{1}{2} m_\chi v_0^2 = \left( \frac{v_0^2}{v^2} \right) E_i \quad \text{with} \quad v_0 = 220 \text{ km} \cdot \text{s}^{-1}$$

and using it in the expression of  $v_{min}$  we get

$$v_{min} = \left( \frac{E_R}{E_0 r} \right)^{1/2} v_0 \quad (2.10)$$

Also,  $E_{min}$  is determined by the escape velocity (i.e.  $v_{max} = v_{esc}$ ) of WIMPs from the Milky Way: we don't expect any WIMPs with a velocity higher than  $544 \text{ km} \cdot \text{s}^{-1}$ . For the derivations here this effect will be ignored, since it does not

affect the results in a qualitative way.

Therefore, equation (2.9) can be written as:

$$\frac{dR}{dE_R} = \frac{1}{E_0 r} \int_{v_{min}}^{v_{max}} \frac{v_0^2}{v^2} dR(v) \quad (2.11)$$

The next step is to find  $dR$ , i.e. the event rate per unit mass on a target of atomic mass  $A$ , with cross-section per nucleus  $\sigma_0$ , which can be written as:

$$dR = \frac{N_A}{A} \sigma_0 v dn, \quad (2.12)$$

where  $N_A$  is the Avogadro number ( $6.02 \times 10^{26} \text{ kg}^{-1}$ ), and  $dn$  is the particle density of WIMP particles with relative velocities within  $d^3v$  about  $v$ . Particle density  $dn$  can be written as:

$$dn = \frac{n_0}{k} f(v, v_E) d^3v \quad (2.13)$$

Here  $k$  is the normalization constant,  $n_0$  is the mean WIMP number density ( $= \frac{\rho_\chi}{m_\chi}$  for dark matter particle mass  $m_\chi$  and density  $\rho_\chi$ ),  $v$  is the velocity of WIMP relative to target (earth) and  $v_E$  is the Earth (target) velocity relative to the dark matter distribution.

To determine the normalization constant  $k$  we integrate this equation over all velocities demanding that we should get the mean number density of WIMPs,  $n_0$ . So:

$$\int_0^{v_{esc}} dn = n_0$$

i.e.,

$$k = \int f(v, v_E) d^3v$$

$$k = \int_0^{2\pi} d\phi \int_{-1}^{+1} d(\cos \theta) \int_0^{v_{esc}} f(v, v_E) v^2 dv$$

Now, it is assumed that the WIMP velocity distribution is as follows:

$$f(v, v_E) = e^{-(v+v_E)^2/v_0^2} \quad (2.14)$$

where  $(v + v_E)$  is the WIMP velocity in the galaxy frame,  $v_0 = 220 \text{ km} \cdot \text{s}^{-1}$  and  $v_{esc}$  is the local galactic escape velocity.

Considering a simplified case in which  $v_{esc} = \infty$  and  $v_E = 0$ , the normalization constant becomes:

$$\begin{aligned}
k &= \int_0^{2\pi} d\phi \int_{-1}^{+1} d(\cos \theta) \int_0^\infty e^{-v^2/v_0^2} v^2 dv \\
&= 4\pi \int_0^\infty e^{-v^2/v_0^2} v^2 dv \\
&= (\pi v_0^2)^{3/2} = k_0
\end{aligned}$$

Therefore, equation (2.12) can be written as:

$$\begin{aligned}
dR &= \frac{N_A}{A} \sigma_0 v \left( \frac{n_0}{k} f(v, v_E) d^3 v \right) \\
&= \frac{N_A}{A} \sigma_0 n_0 \frac{k_0}{(\pi v_0^2)^{3/2} k} v f(v, v_E) d^3 v \\
&= \frac{k_0}{k} \left( \frac{2}{\sqrt{\pi}} \frac{N_A}{A} \frac{\rho_\chi}{m_\chi} \sigma_0 v_0 \right) \frac{\sqrt{\pi}}{2v_0} \frac{1}{\pi^{3/2} v_0^3} v f(v, v_E) d^3 v \\
&= \frac{k_0}{k} R_0 \frac{1}{2\pi v_0^4} v f(v, v_E) d^3 v \tag{2.15}
\end{aligned}$$

Here  $R_0$ , is defined as the total event rate per unit mass for  $v_E = 0$  and  $v_{esc} = \infty$ , i.e.

$$R_0 = \frac{2}{\sqrt{\pi}} \frac{N_A}{A} \frac{\rho_\chi}{m_\chi} \sigma_0 v_0 \tag{2.16}$$

Using equation (2.15) in (2.11) we get:

$$\frac{dR}{dE_R} = \frac{R_0}{E_0 r} \frac{k_0}{k} \frac{1}{2\pi v_0^2} \int_{v_{min}}^{v_{max}} \frac{1}{v} f(v, v_E) d^3 v \tag{2.17}$$

Evaluating the above expression for  $v_E = 0$  and  $v_{esc} = \infty$ , we will get

$$f(v, v_E) = e^{-v^2/v_0^2} \quad \text{and} \quad \frac{k_0}{k} = 1$$

and equation (2.17) becomes:

$$\begin{aligned}
\frac{dR}{dE_R}(0, \infty) &= \frac{R_0}{E_0 r} \frac{1}{2\pi v_0^2} \int_{v_{min}}^{\infty} \frac{1}{v} e^{-v^2/v_0^2} 4\pi v^2 dv \\
&= \frac{R_0}{E_0 r} \frac{2}{v_0^2} \int_{v_{min}}^{\infty} e^{-v^2/v_0^2} v dv \\
&= \frac{R_0}{E_0 r} \left( - \left[ e^{-v^2/v_0^2} \right]_{v_{min}}^{\infty} \right) \\
&= \frac{R_0}{E_0 r} e^{-v_{min}^2/v_0^2}
\end{aligned}$$

Finally, using the expression for  $v_{min}$  from equation (2.10), the expression for the differential event rate can be written as:

$$\frac{dR}{dE_R}(0, \infty) = \frac{R_0}{E_0 r} e^{-E_R/E_0 r} \quad (2.18)$$

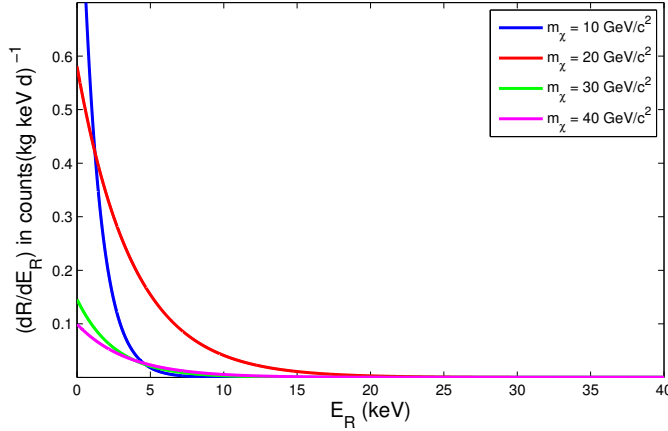


**Figure 2.5:** Event rate dependence on WIMP mass for Germanium as target material.

From Figure 2.5, it can be observed that Recoil spectrum gets shifted to low energies for low - mass WIMPs. Also, one needs a light target and/or a low threshold to detect a low mass WIMP, i.e lower the detector threshold, better the chances of observing an event.

## 2.4 WIMP-Nucleon cross section

In our equation for interaction rate there is  $R_0$  defined earlier as:

$$R_0 = \frac{N_A \rho_\chi}{A m_\chi} \sigma_0 \langle v \rangle$$

with all the particle physics hidden inside  $\sigma_0$ , which is the cross section for the process of WIMP colliding with the nucleus. We will now write this  $\sigma_0$  in terms of WIMP-nucleon cross section.

Let us look at the differential cross section as a function of momentum transfer( $q^2$ ). Starting with the identity:

$$\sigma_0 = \int \frac{d\sigma_0}{dq^2} dq^2$$

The reason to calculate  $\frac{d\sigma_0}{dq^2}$  is that we have a fundamental identity from particle physics relating differential cross section to the quantum mechanical matrix element,  $\mathcal{M}$ . This identity is known as "Fermi's Golden rule":

$$\frac{d\sigma_0}{dq^2} = \frac{1}{\pi v^2} |\mathcal{M}|^2 \quad (2.19)$$

where  $v$  is the WIMP velocity relative to the target, and  $|\mathcal{M}|^2$  represents the 'probability' for a process to occur, which in our case is the scattering of a WIMP to a nucleus.

In the  $q \rightarrow 0$  limit, ie under the assumption of coherent scattering (De Broglie wavelength corresponding to the momentum transfer is similar or larger in size to a nucleus.), we can write  $\mathcal{M}$  as:

$$\mathcal{M} = Z f_p + (A - Z) f_n$$

where  $Z$  is the number of protons,  $A - Z$  is the number of neutrons and we denote the coupling to either a proton or a neutron by  $f_p$  and  $f_n$ , respectively.

Therefore, we can write

$$\left. \frac{d\sigma_0}{dq^2} \right|_{q \rightarrow 0} = \frac{1}{\pi v^2} [Z f_p + (A - Z) f_n]^2$$

A standard cross section  $\sigma_0^{SI}$  is defined as the total cross section at zero momentum transfer:

$$\begin{aligned}\sigma_0^{SI} &= \int_0^{4\mu_T^2 v^2} \left. \frac{d\sigma_0}{dq^2} \right|_{q \rightarrow 0} dq^2 \\ &= \frac{4\mu_T^2}{\pi} [Zf_p + (A-Z)f_n]^2\end{aligned}\quad (2.20)$$

where  $4\mu_T^2 v^2$  is the momentum transfer at  $E_R = E_R^{max}$ .

Considering ( $f_p \simeq f_n$ ), above equation reduces to

$$\sigma_0^{SI} = \frac{4\mu_T^2}{\pi} A^2 f_p^2 \quad (2.21)$$

Now, the spin-independent WIMP scattering cross-section with a single proton can be written as (with  $A = 1$ )

$$\sigma_p^{SI} = \frac{4\mu_p^2}{\pi} f_p^2 \quad (2.22)$$

where  $\mu_p$  is the reduced mass of WIMP-proton system. Combining equations 2.21 and 2.22 we will get

$$\sigma_0^{SI} = \left( \frac{\mu_T}{\mu_p} A \right)^2 \sigma_p^{SI} \quad (2.23)$$

The SI WIMP nucleus scattering cross-section is larger than the SI WIMP-nucleon cross-section by an amount  $\left( \frac{\mu_T}{\mu_p} A \right)^2$ , which is different for different target nuclei (different  $A$ ). But we see that SI WIMP-nucleon cross-section is model independent and also independent of the scattered nucleus and hence the target material. The dark matter direct detection experiments obtain limits on  $\sigma_p^{SI}$  vs  $m_\chi$ . Thus results are given in terms of target independent quantity  $\sigma_p^{SI}$ .

## 2.5 Nuclear Form Factor

In the previous section we have treated the nucleus as a point object and therefore we could justify the assumption of coherent scattering of a WIMP. As the energy

of the recoil increases,  $q > 0$ , the WIMP begins to probe the internal structure of the nucleus and the interaction loses coherence. This loss is parameterized by a nuclear form factor  $F(q)$  to account for the finite size of the nucleus, where  $F(q = 0) = 1$ .

$$\sigma_0^{SI} = \left( \frac{\mu_T}{\mu_p} A \right)^2 \sigma_p^{SI} F^2(q)$$

We see that WIMP nucleus cross section no longer depends on  $A^2$  and the effective cross section decreases when  $F(q) < 1$ .

The nuclear form factor,  $F(q)$ , is taken to be the Fourier transform of  $\rho(r)$ , the density distribution of the scattering centres.

$$\begin{aligned} F(q) &= \int \rho(r) e^{iq \cdot r} d^3r \\ &= \int_0^{2\pi} d\phi \int_0^\infty r^2 \rho(r) dr \int_0^\pi e^{iqr \cos \theta} \sin \theta d\theta \\ &= \frac{4\pi}{q} \int_0^\infty r \sin(qr) \rho(r) dr. \end{aligned} \tag{2.24}$$

There are several analytical and theoretical models for the form factor[13], the distribution proposed by Helm[3] is most commonly used in dark matter calculations/simulations given by:

$$\begin{aligned} F(q) &= 3 \frac{j_1(qr_n)}{qr_n} e^{-\frac{1}{2}(qs)^2} \\ &= 3 \frac{\sin(qr_n) - qr_n \cos(qr_n)}{(qr_n)^3} e^{-\frac{1}{2}(qs)^2}, \end{aligned}$$

where  $j_1$  is the spherical Bessel function of the first order,  $s$  is the measure of the nuclear skin thickness, and  $r_n$  is the effective nuclear radius. There are several methods of parameterizing these values[7].

To arrive to the above result, first we assume a uniform charge distribution, up to some radius  $r_n$ , radius of the nucleus. In this case, the normalized density takes

the form:

$$\rho_U(r) = \frac{3}{4\pi(r_n)^3} \Theta(R-r) \quad (2.25)$$

Thus, combining equation (2.24) and (2.25), gives, after some reorganization:

$$F_U(q) = \frac{3}{(qr_n)^3} \int_0^{qr_n} z \sin(z) dz$$

which gives

$$F_U(q) = 3 \frac{\sin(qr_n) - qr_n \cos(qr_n)}{(qr_n)^3} \quad (2.26)$$

But such a charge density is nonphysical because a nucleus cannot have such a sharp cutoff in its charge distribution. This problem is solved by convoluting the uniform charge density with a Gaussian “surface smearing” density given as:

$$\rho_G(r) = \frac{1}{(2\pi s^2)^{3/2}} e^{-r^2/2s^2}, \quad (2.27)$$

where  $s$  is a measure of nuclear skin thickness.

Substituting equation (2.27) in (2.24), we get

$$F_G(q) = \frac{4\pi}{q} \int_0^\infty r \sin(qr) \left( \frac{1}{(2\pi s^2)^{3/2}} e^{-r^2/2s^2} \right) dr$$

$$F_G(q) = \frac{4\pi}{q} \frac{1}{(2\pi s^2)^{3/2}} \int_0^\infty r e^{-r^2/2s^2} \frac{(e^{iqr} - e^{-iqr})}{2i} dr$$

$$F_G(q) = \frac{4\pi}{q} \frac{1}{(2\pi s^2)^{3/2}} \frac{1}{2i} \left[ \int_0^\infty r e^{-\frac{r^2}{2s^2} + iqr} dr - \int_0^\infty r e^{-\frac{r^2}{2s^2} - iqr} dr \right]$$

using the following identity

$$\int_{-\infty}^\infty e^{(-ax^2+bx)} = e^{b^2/4a} \sqrt{\frac{\pi}{a}}$$

we get

$$\int_0^{\infty} e^{-\frac{r^2}{2s^2} + iqr} = \int_0^{\infty} e^{-\frac{r^2}{2s^2} - iqr} = \frac{1}{2}(\sqrt{\pi 2s^2})e^{-\frac{q^2 s^2}{2}}$$

Therefore

$$F_G(q) = \frac{4\pi}{q} \frac{1}{(2\pi s^2)^{3/2}} \frac{1}{2i} \frac{1}{2} \left[ \frac{1}{i} \frac{d}{dq} (\sqrt{\pi 2s^2} e^{-\frac{q^2 s^2}{2}}) - \frac{1}{-i} \frac{d}{dq} (\sqrt{\pi 2s^2} e^{-\frac{q^2 s^2}{2}}) \right]$$

$$F_G(q) = \frac{4\pi}{q} \frac{1}{(2\pi s^2)^{3/2}} \frac{1}{2i} \frac{1}{2} \frac{1}{i} \sqrt{\pi 2s^2} (-2qs^2 e^{-\frac{q^2 s^2}{2}})$$

$$F_G(q) = e^{-\frac{q^2 s^2}{2}} \quad (2.28)$$

By the convolution theorem, the form factor is simply a product of the form factors of  $\rho_U$  and  $\rho_G$  [15]. Therefore combining equations (2.26) and (2.28):

$$\begin{aligned} F(q) &= F_U(q)F_G(q) \\ &= 3 \frac{\sin(qr_n) - qr_n \cos(qr_n)}{(qr_n)^3} e^{-\frac{1}{2}(qs)^2} \end{aligned} \quad (2.29)$$

The squares of the Helm form factor for various target with  $r_n = 1.2A^{1/3}$  and  $s = 1$  fm are shown in Figure 2.6.

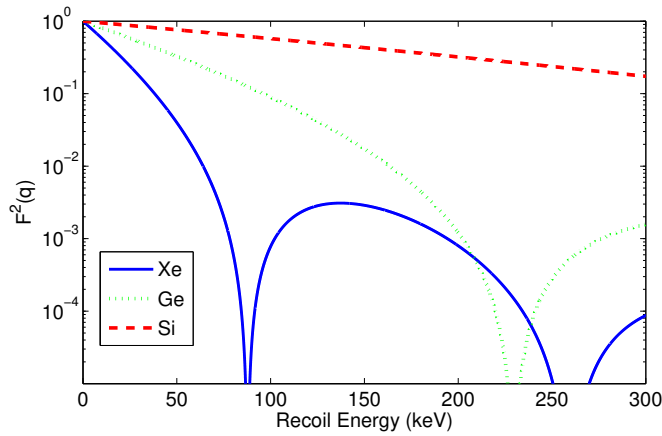


**Figure 2.6:** Helm form factor as a function of nuclear recoil energy for different target: Xe (blue solid), Ge (green dotted), and Si (red dashed)

Figure 2.6 shows loss of coherence as larger momentum transfers probes smaller scales. The nuclear form factor has a significant effect on the recoil rates for heavier targets.

Now, equation 2.18 can be modified as:

$$\frac{dR}{dE_R}(0, \infty) = \frac{R_0}{E_0 r} e^{-E_R/E_0 r} F^2(q) \quad (2.30)$$

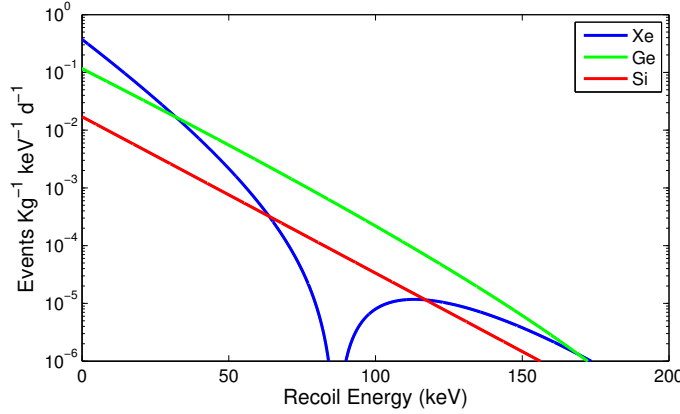


**Figure 2.7:** Variation of Recoil Energy spectrum with  $A$  for  $m_\chi = 100 \text{ GeV}/c^2$

From Figure 2.7 it is clear that the change in the energy dependence is especially critical because detectors have thresholds in the few-to-tens-of-keV region. A germanium target offers a clear advantage over a silicon target, but Xe yields no benefit over germanium unless the recoil-energy threshold is below 20 keV.

## 2.6 Correction in event rate due to Earth's velocity

The differential recoil energy spectrum is expressed as:

$$\frac{dR}{dE_R}(v_E, v_{esc}) = \frac{R_0}{E_0 r} \frac{k_0}{k} \frac{1}{2\pi v_0^2} \int_{v_{min}}^{v_{max}} \frac{1}{v} f(v, v_E) d^3 v$$

To correctly evaluate the integral on the velocity, it has to be considered that the WIMP velocity in the galactic reference frame,  $v'$ , cannot exceed  $v_{esc}$  otherwise DM particles would escape from the galaxy. The velocity  $v'$  is composition of the WIMP velocity relative to the target,  $v$ , and velocity of the target itself:  $v' = v_E + v$ .

Its module is given by:  $v'^2 = v^2 + v_E^2 + 2vv_E \cos \theta$ . Here  $\theta$  is the scattering angle in the galactic rest frame. It means that:  $(v - v_E)^2 \leq v'^2 \leq (v + v_E)^2$ , thus setting a certain value for  $v$ ,  $v'$  results function of  $\cos \theta$ . It should be noted that the integral in above equation is evaluated on the WIMP relative velocity,  $v$ . The maximum value of  $v$  is reached when the Earth moves in the opposite direction with respect to the incoming WIMP when the latter has  $v' = v_{esc} : v_{max} = v' + v_E$ . Now, two cases have to be considered:

- if  $v \leq v_{esc} - v_E$ , then it is possible to integrate equation without any condition on  $\cos \theta$ , since it always results  $v' \leq v_{esc}$ :  

$$v'^2 = (v + v_E)^2 \leq (v_{esc} - v_E + v_E)^2 \leq v_{esc}^2;$$
- if  $v_{esc} - v_E \leq v \leq v_{esc} + v_E$ , then it has to be set a condition on  $\cos \theta$ :  $v'^2 = v^2 + v_E^2 + 2vv_E \cos \theta \leq v_{esc}^2 \implies \cos \theta \leq (v_{esc}^2 - v^2 - v_E^2)/2vv_E$ .

The integral on the velocity becomes:

$$\begin{aligned} \int_{v_{min}}^{v_{max}} \frac{1}{v} f(v, v_E) d^3 v &= \int_0^{2\pi} d\phi \int_{-1}^{C_{max}} d(\cos \theta) \int_{v_{min}}^{v_{esc}} \frac{1}{v} f(v, v_E) dv \\ &= 2\pi \left[ \int_{-1}^1 d(\cos \theta) \int_{v_{min}}^{v_{esc} - v_E} + \int_{-1}^{(v_{esc}^2 - v^2 - v_E^2)/2vv_E} d(\cos \theta) \int_{v_{esc} - v_E}^{v_{esc} + v_E} \right] \frac{1}{v} f(v, v_E) dv \end{aligned}$$

The lower bound of the integral on  $\cos \theta$  can be leaved equal to -1 since the physical condition  $v' \geq 0$  is always satisfied. Besides the conditions on  $\cos \theta$ , it has to be considered also a condition on  $v_{min}$  to assure that  $v_{min} \leq v_{esc} - v_E$ . If this relation is not satisfied, one should consider only the second part of the last integral in equation, substituting the lower bound of the velocity integral with  $v_{min}$ , otherwise the integral is evaluated with the wrong condition on the  $\cos \theta$ . Thus, the integral on the velocity can be written as:

$$\int_{v_{min}}^{v_{max}} \frac{1}{v} f(v, v_E) d^3 v = 2\pi \times \begin{cases} \left[ \int_{-1}^1 \int_{v_{min}}^{v_{esc} - v_E} + \int_{-1}^{(v_{esc}^2 - v^2 - v_E^2)/2vv_E} \int_{v_{esc} - v_E}^{v_{esc} + v_E} \right] \frac{1}{v} f(v, v_E) d(\cos \theta) dv & \text{for } 0 \leq v_{min} \leq v_{esc} - v_E \\ \int_{-1}^{(v_{esc}^2 - v^2 - v_E^2)/2vv_E} \int_{v_{min}}^{v_{esc} + v_E} \frac{1}{v} f(v, v_E) d(\cos \theta) dv & \text{for } v_{esc} - v_E \leq v_{min} \leq v_{esc} + v_E \\ 0 & \text{for } v_{min} \geq v_{esc} + v_E \end{cases}$$

Using the conditions on  $\cos \theta$  and  $v_{min}$ , it is possible to integrate equation. The expected DM differential energy spectrum, for various assumptions about  $v_E$  and  $v_{esc}$ , is thus given by:

$$\frac{dR}{dE_R}(0, \infty) = \frac{R_0}{E_0 r} e^{-E_R/E_0 r} \quad (2.31)$$

$$\frac{dR}{dE_R}(0, v_{esc}) = \frac{k_0}{k_1} \left[ \frac{dR}{dE_R}(0, \infty) - \frac{R_0}{E_0 r} e^{-v_{esc}^2/v_0^2} \right] \quad (2.32)$$

$$\frac{dR}{dE_R}(v_E, \infty) = \frac{R_0}{E_0 r} \frac{\sqrt{\pi}}{4} \frac{v_0}{v_E} \left[ erf \left( \frac{v_{min} + v_E}{v_0} \right) - erf \left( \frac{v_{min} - v_E}{v_0} \right) \right] \quad (2.33)$$

$$\frac{dR}{dE_R}(v_E, v_{esc}) = \frac{k_0}{k_1} \left[ \frac{dR}{dE_R}(v_E, \infty) - \frac{R_0}{E_0 r} e^{-v_{esc}^2/v_0^2} \right] \quad (2.34)$$

where ,

$$erf(x) = \frac{2}{\sqrt{\pi}} \int_0^x e^{-t^2} dt$$

$$k_1 = k_0 \left[ erf \left( \frac{v_{esc}}{v_0} \right) - \frac{2}{\sqrt{\pi}} \frac{v_{esc}}{v_0} e^{-v_{esc}^2/v_0^2} \right]$$

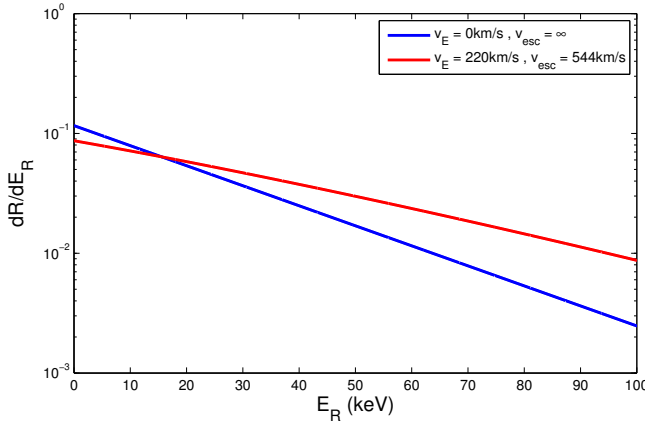


**Figure 2.8:** The effect of the movement of the earth through the galaxy on the recoil rate

In Figure 2.8 the effect of movement of earth on the recoil rate has been calculated for a WIMP with a mass of  $100 GeV/c^2$  interaction with a nucleus with

$m_T = 68.036 \text{ GeV}/c^2$  (i.e. Germanium). The blue line shows the rate if the earth would be at rest in the galactic coordinate frame (i.e. non rotation around the galactic center), while the red line shows the spectrum you obtain if the sun is moving with 220 km/s as it does. This slightly helps dark matter experiments increase their sensitivity. Also the finite escape velocity is taken into account, although the effect is small.

The Earth's orbit about the Sun leads to a time dependence, specifically an annual modulation, in the differential event rate. The Earth's speed with respect to the Galactic rest frame is largest in summer when the component of the Earth's orbital velocity in the direction of solar motion is largest. Therefore the number of WIMPs with high (low) speeds in the detector rest frame is largest (smallest) in summer. Consequently the differential event rate has an annual modulation, with a peak in winter for small recoil energies and in summer for larger recoil energies. The effect to the rate can be approximated as [14]:

$$\frac{dR}{dE_R}(E_R, t) \approx \frac{dR}{dE_R}(E_R) \left( 1 + \Delta(E_R) \cos \left( 2\pi \frac{t - t_0}{T} \right) \right)$$

The period of the oscillation will be one year  $T = 1$  year and the rate will be maximum at  $t$  corresponding to June 2nd. The amplitude is 1-10% percent, but it allows a measurement of dark matter with an intrinsic way of suppressing backgrounds. Some experiments exploit the effect of the change in amplitude – resulting in a change of event rate – as a way to subtract all constant background sources that do not show a seasonal effect. One of the most famous claims of dark matter discovery made by the DAMA/LIBRA collaboration is based on a seasonal effect in detector counting rates.

## 2.7 Direct Detection techniques

The recoil energy due to a possible impact of dark matter is detected in a detector mainly by three processes that the recoil nucleus would undergo inside the detector. They are phonons, ionization, and scintillation.

•**Phonons:** A phonon is a collective excitation of the crystal in which the periodic arrangement in the crystal is set to vibrational mode (normal mode) at a single frequency. In the case of materials (such as Ge) chosen for dark matter detection, the multiple collisions of the recoil nucleus convert the kinetic energy

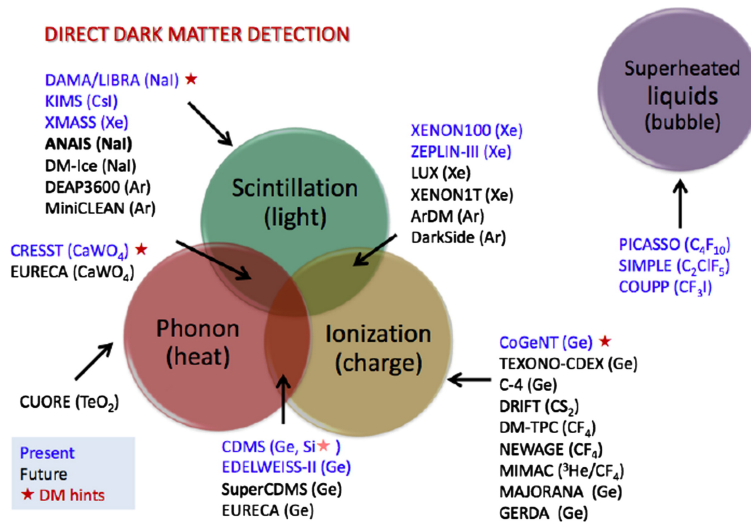


**Figure 2.9:** Experimental approaches for direct dark matter detection.

into collective excitation of the crystal. The resulting phonon vibration increases the temperature of the crystal which is measured.

●**Scintillation:** Scintillation is a phenomenon in which the incident particles or photons excite atoms or molecules in the ground state and the light is reemitted when the atom comes down to the initial state again – in other words the absorbed energy is reemitted (luminescence). In a crystal, the electrons are elevated from the valence band to the conduction band and populate this latter band. When they come down again to the valence band, the scintillation is emitted. In a dark matter scintillator detector, the nuclear recoil energy produces the scintillation effect and the scintillation signal in fact gives a measure of the recoil energy imparted to the recoiling nucleus.

●**Ionization:** Ionization is the process by which electrons are ejected from the target atom. These electrons can be separated from the positive ion by applying an electric field over the target. There is an intricate interplay between the ionization and scintillation process: separating the charges with an electric charge leaves fewer possibilities for charge recombination processes causing scintillation light.

Fig. 2.9 shows a summary of present and future experiments, indicating the techniques used in each case.

# Chapter 3

## Dark Matter exclusion limits

In order to search for new physics phenomena or particles, one must distinguish between background (already known physics) and signal (new physics) events, and then study through statistical concepts the possible hypotheses at stake, basically the null or background-only hypothesis  $H_0$  (which describes only known processes) and an alternative hypothesis  $H_1$  (which includes both background and new physics signals).

Searches for rare events, like Dark Matter interactions with nucleons, often lead to the observation of no signal-type events, or the observed ones are compatible with the background-only hypothesis, and what an experiment is able to set is an upper limit for the quantity related to the appearance of new physics events. In our case such a quantity is the WIMP-nucleon cross section, as a function of the possible WIMP masses.

The usual method to obtain an upper limit at some confidence level is to vary the theoretical parameters until the appropriate cumulative probability distribution function (CDF) takes on the confidence level desired (0.9 for a 90% confidence level upper limit) when evaluated at the observed statistic (e.g. the number of observed events).

### 3.1 Poisson Method

Consider a series of nuclear recoil energy measurements  $E_1, \dots, E_N$  where  $N$  is the total number of measurements. Assume the data points are distributed with a known theoretical function  $dN/dE$ . To set a limit, we are interested in the probability, given a value of the cross section  $\sigma$  in a theoretical distribution  $dN/dE$ , that the total number of events observed in our data is equal to a certain value or less.

The probability of finding an observed number of events  $N_{obs}$  given an expected number of events  $\mu$  is given by Poisson distribution:

$$P(N = N_{obs}) = \frac{e^{-\mu} \mu^{N_{obs}}}{N_{obs}!}$$

Also,

$$P(N \leq N_{obs}) = \sum_{n=0}^{N_{obs}} \frac{e^{-\mu} \mu^n}{n!}$$

- Example:

Suppose  $N_{obs} = 0$ , then What is the 95% CL limit on  $\mu$ ?

we have  $P(N \leq 0) = e^{-\mu}$ , then find  $\mu$  such that

$$P(N \leq 0) = 1 - CL \implies \mu > -\ln(1 - CL)$$

Therefore, for  $N_{obs} = 0$  and  $CL = 0.95$ , exclude  $\mu > 3$

Now, In our case if we are conservative and assume no knowledge of the background distribution and therefore that all observed events are signal, then an upper limit at some desired confidence level may be set by adjusting  $\sigma$  in  $dN/dE$  until the total number of events  $\mu$  expected, given by integrating  $dN/dE$  over the whole experimental range, is such that it satisfies the following equation

$$\alpha = e^{-\mu} \sum_{n=0}^{N_{obs}} \frac{\mu^n}{n!}$$

where  $1 - \alpha$  is the confidence level of the upper limit set in this way, and  $N_{obs}$  is the number of observed data events.

### 3.2 Maximum Gap method

The Maximum Gap is a statistical method [9] used to quote upper limits, with a certain confidence level (CL), of the  $\sigma$  for WIMP-nucleon scatterings when:

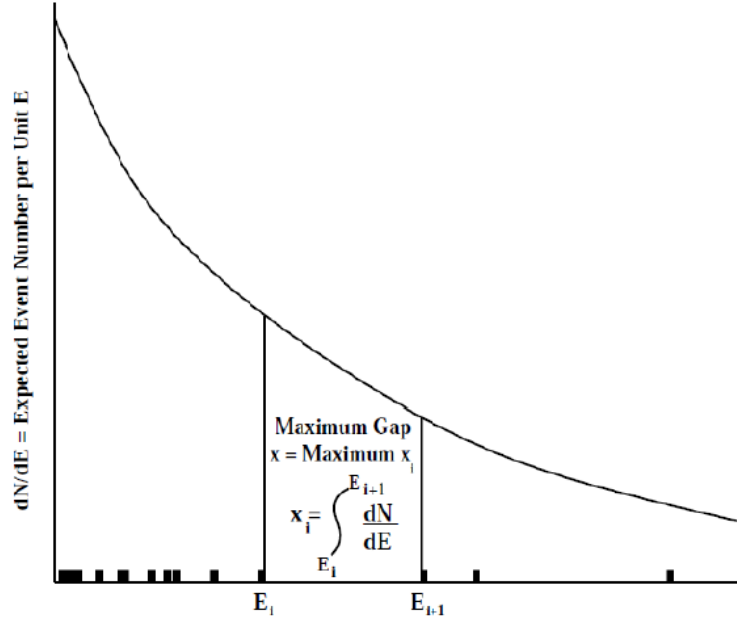


**Figure 3.1:** Explanation of the Maximum Gap method

- there are no clear evidences for a signal event;
- there is the possibility for the existence of an unknown background;
- the observed events are compatible with the background-only hypothesis.

From the DM theory it is possible to obtain the shape of the expected WIMP recoil energy spectra, but not their normalization, i.e. the  $\sigma$ . The procedure to use the Maximum Gap method can be schematically summarized as in Figure 3.1. In Figure 3.1, the  $dN/dE$  curve represents the expected signal spectrum for which one wants to evaluate the cross section, while the black rectangles are the observed events. On the  $x$ -axis there is the energy of the recoils, but any other 1-D variable can be used. Assuming a certain value for the cross section, between each two consecutive events there is a "gap" given by:

$$x_i = \int_{E_i}^{E_{i+1}} \frac{dN}{dE} dE$$

where  $E_{i,i+1}$  are the energies of any two adjacent events. The gap sizes  $x_i$  represent the number of expected signal events, for the hypothesized value of the  $\sigma$ , in energy intervals where no events have been observed. Given a certain distribution

for the data, the "maximum gap" is the largest gap between them. The procedure to apply the method can be summarized as follows: Suppose to have, as result of a simulated experiment, a certain number of events that are distributed following a certain 1-D variable, like the recoil energy. Then, it is assumed that all the events are due only to the background, being interested in upper limits in the background-only hypothesis. Between each two adjacent events we evaluate, using the signal spectrum, the size of the gap and then we look for the largest one. The gaps are evaluated on the signal spectrum because one wants to quote upper limits for the signal cross section. Thus, the gaps represent the number of signal events that we were expecting to observe, for the assumed value of the  $\sigma$ , between two adjacent background events. Knowing the maximum gap and having observed 0 events in it, we want to know the value of the  $\sigma$  for which we would observed 0 events with a certain probability. The value of the probability defines the CL of the upper limit. Finally, the Maximum Gap method returns the value of the cross section that is the upper limit on this parameter, with the desired CL ( $\sigma^{CL}$ ). This procedure shields against regions where the background gives many events, as the low energy part of the spectrum, since it is not probable to find the maximum gap there. In this way, the method is naturally applied in region where the background has not a large impact on the detector sensitivity.

This is a recursive method where one tries and rejects different values of the  $\sigma$

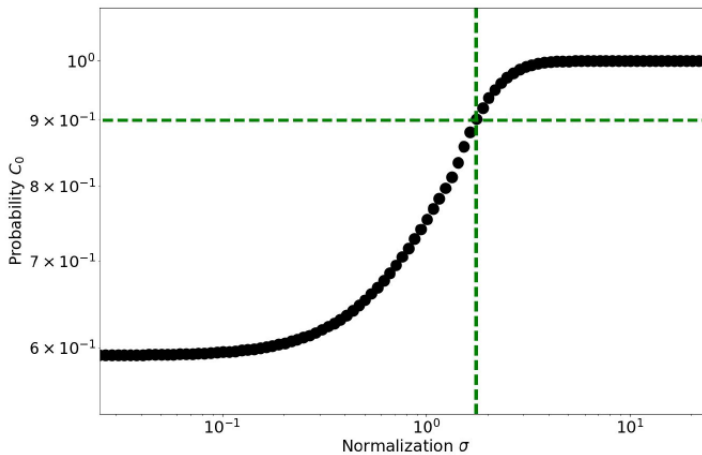


**Figure 3.2:** Finding 90%  $\sigma^{CL}$  for a particular  $m_\chi$

until the one that satisfy the CL condition is found. Very large values of the cross section can a priori be excluded since it is not probable to observe zero events in gaps which provide a huge number of expected recoils. Going towards low

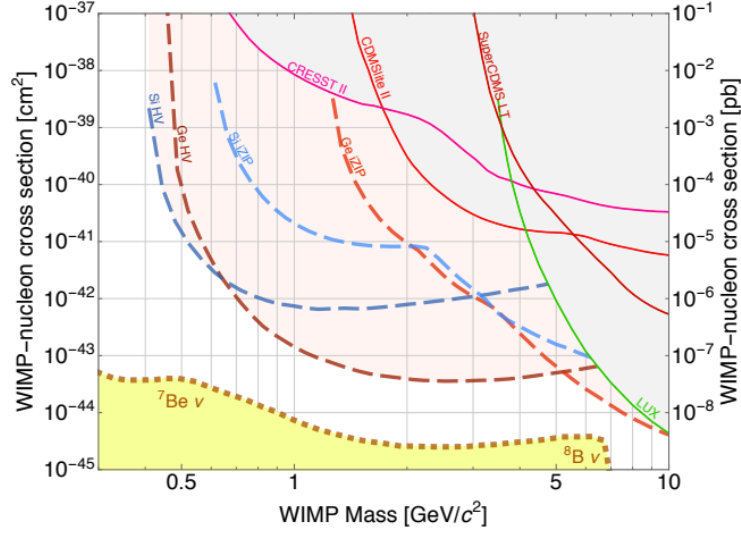


**Figure 3.3:** Projected exclusion sensitivity for the SuperCDMS SNOLAB direct detection dark matter experiment along with current experimental exclusion limits from various experiments. Figure taken from [19]

values for the  $\sigma$  it is necessary to define a criterion to decide if a certain value can be accepted or rejected. Assuming a certain hypothesis on  $\sigma$  being the correct value, one could reject it, as too high, if random experiments would almost always observe less events in their maximum gap. Thus, the procedure simply compare different hypothesis on the signal strength and returns, as upper limit, the one that gives with  $C_0$  probability a lower number of expected events compared with the observed one. Being  $X$  the observed maximum gap, if the probability to observe a lower value for  $x$  (the random maximum gap) is  $C_0$ , then one can reject the hypothesized value of the cross section with a  $CL$  of  $C_0$ . The probability  $C_0$  is given by [9]

$$C_0(x, \mu) = \sum_{k=0}^m \frac{(kx - \mu)^k e^{-kx}}{k!} \left( 1 + \frac{k}{\mu - kx} \right) \quad (3.1)$$

where  $\mu$  is the total number of the expected signal events, i.e. the integral of the dark matter recoil energy spectrum over the whole energy range,  $x$  is the maximum gap and  $m$  is the largest integer  $\leq \mu/x$ . The value of the cross section at a certain  $CL$  is obtained by applying a recursive procedure to equation 3.1 until  $C_0 = CL$ .

The above procedure for finding a 90% upper  $CL$  on  $\sigma$  for a fixed WIMP mass is shown in Figure 3.2. The same procedure can be looped over certain

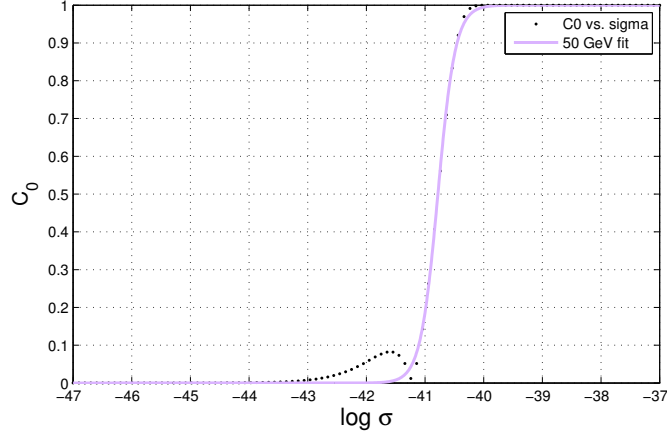


**Figure 3.4:** Finding 90% CL on  $\sigma$  for  $50 \text{ GeV}/c^2 \text{ mass}$

WIMP mass range. Finally what we get is a plot between  $\sigma$  (WIMP-nucleon cross-section) vs  $m_\chi$  known as exclusion plot (or sensitivity curve of an experiment).

Figure 3.3 shows the projected exclusion sensitivity for the upcoming direct detection dark matter experiment SuperCDMS SNOLAB along with current experimental exclusion limits from various experiments in the low-mass region such as CRESST-II and LUX. The dotted orange line is the dark matter discovery limit.

### 3.2.1 Result

Maximum gap method was applied to a given set of observed events. First, for a fixed  $m_\chi$ ,  $C_0$  vs  $\sigma$  was plotted. Then 90% CI limit on  $\sigma$  was interpolated ( $C_0 = 0.9$ ) by fitting the data points of  $m_\chi$ ,  $C_0$  vs  $\sigma$  with sigmoid function (as shown in Fig 3.4 for  $m_\chi = 50 \text{ GeV}/c^2$ ). Same process was repeated for different masses. 90% CI limit on  $\sigma$  for different masses is shown in Table 3.1.

WIMP mass ( $GeV/c^2$ )	$\log_{10}\sigma$
50	-40.4527
55.05	-40.3972
60.60	-40.3211
65.15	-40.2720
70.20	-40.2157
75.25	-40.1692
80.80	-40.1176
85.85	-40.0726
90.40	-40.0297

**Table 3.1:** Upper CL limit on  $\sigma$  for different WIMP masses

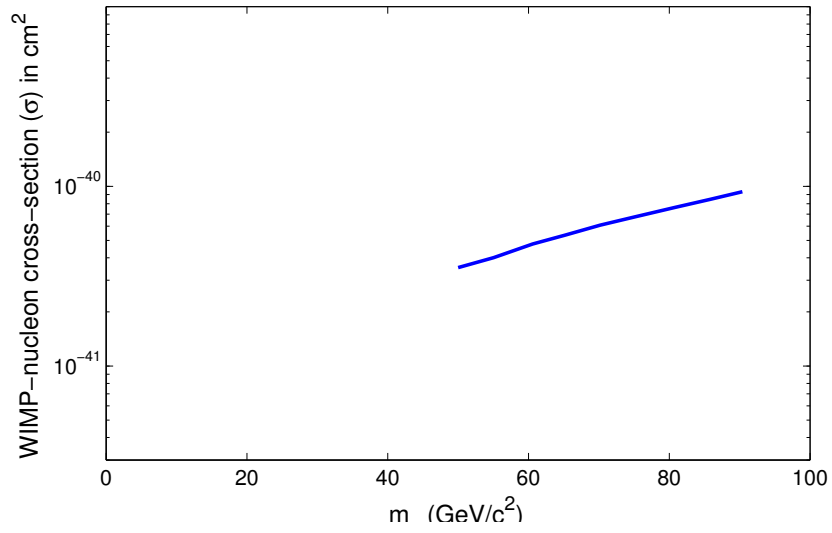


**Figure 3.5:** WIMP-nucleon cross-section ( $\sigma$ ) vs WIMP mass ( $m_\chi$ )

# Acknowledgement

I am extremely grateful to the Science Academies - Indian Academy of Sciences(IAS), Indian National Science Academy(INSA) and the National Academy of Sciences, India(NASI) for granting me the Summer Research Fellowship,2018 to carry out this project. Further, I would like to thank my guide Prof. Bedan-gadas Mohanty for guiding me through the project. I would also like to thank Rik Bhattacharyya, Vijay Iyer and Samir Banik for all the discussions and helping me throughout my period of stay in NISER.

# Bibliography

- [1] Fritz Zwicky. “Die rotverschiebung von extragalaktischen nebeln”. In: *Helvetica Physica Acta* 6 (1933), pp. 110–127.
- [2] Fritz Zwicky. “On the Masses of Nebulae and of Clusters of Nebulae”. In: *The Astrophysical Journal* 86 (1937), p. 217.
- [3] Richard H Helm. “Inelastic and elastic scattering of 187-MeV electrons from selected even-even nuclei”. In: *Physical Review* 104.5 (1956), p. 1466.
- [4] Vera C Rubin and W Kent Ford Jr. “Rotation of the Andromeda nebula from a spectroscopic survey of emission regions”. In: *The Astrophysical Journal* 159 (1970), p. 379.
- [5] Vera C Rubin, W Kent Ford Jr, and Norbert Thonnard. “Rotational properties of 21 SC galaxies with a large range of luminosities and radii, from NGC 4605/R= 4kpc/to UGC 2885/R= 122 kpc”. In: *The Astrophysical Journal* 238 (1980), pp. 471–487.
- [6] KG Begeman, AH Broeils, and RH Sanders. “Extended rotation curves of spiral galaxies: Dark haloes and modified dynamics”. In: *Monthly Notices of the Royal Astronomical Society* 249.3 (1991), pp. 523–537.
- [7] JD Lewin and PF Smith. “Review of mathematics, numerical factors, and corrections for dark matter experiments based on elastic nuclear recoil”. In: *Astroparticle Physics* 6.1 (1996), pp. 87–112.
- [8] Joakim Edsjö and Paolo Gondolo. “Neutralino relic density including coannihilations”. In: *Physical Review D* 56.4 (1997), p. 1879.
- [9] Steven Yellin. “Finding an upper limit in the presence of an unknown background”. In: *Physical Review D* 66.3 (2002), p. 032005.
- [10] Ofer Lahav and Andrew R Liddle. “The cosmological parameters”. In: *arXiv preprint astro-ph/0406681* (2004).

- [11] Maxim Markevitch et al. “Direct constraints on the dark matter self-interaction cross section from the merging galaxy cluster 1E 0657–56”. In: *The Astrophysical Journal* 606.2 (2004), p. 819.
- [12] Douglas Clowe et al. “A direct empirical proof of the existence of dark matter”. In: *The Astrophysical Journal Letters* 648.2 (2006), p. L109.
- [13] Gintaras Dūda, Ann Kemper, and Paolo Gondolo. “Model-independent form factors for spin-independent neutralino–nucleon scattering from elastic electron scattering data”. In: *Journal of Cosmology and Astroparticle Physics* 2007.04 (2007), p. 012.
- [14] David G Cerdeno and Anne M Green. “Direct detection of WIMPs”. In: *arXiv preprint arXiv:1002.1912* (2010).
- [15] Herbert Uberall. *Electron Scattering From Complex Nuclei V36A*. Vol. 36. Academic Press, 2012.
- [16] CL Bennett et al. “Nine-year Wilkinson Microwave Anisotropy Probe (WMAP) observations: final maps and results”. In: *The Astrophysical Journal Supplement Series* 208.2 (2013), p. 20.
- [17] N Aghanim et al. “Planck 2015 results-XI. CMB power spectra, likelihoods, and robustness of parameters”. In: *Astronomy & Astrophysics* 594 (2016), A11.
- [18] Mark David Pepin. “Low-Mass Dark Matter Search Results and Radiogenic Backgrounds for the Cryogenic Dark Matter Search”. PhD thesis. University of Minnesota, 2016.
- [19] R Agnese et al. “Projected Sensitivity of the SuperCDMS SNOLAB experiment”. In: *Physical Review D* 95.8 (2017), p. 082002.
- [20] Edward Kolb. *The early universe*. CRC Press, 2018.